Provided for non-commercial research and education use.
Not for reproduction, distribution or commercial use.

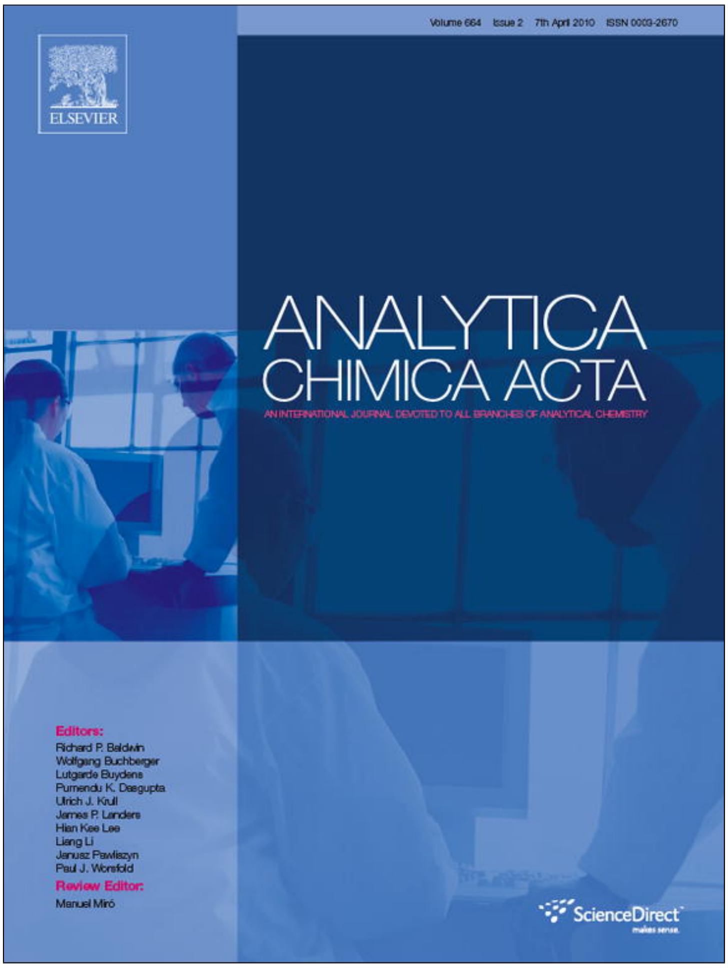
Volume 664 Issue 2 7th April 2010 ISSN 0003-2670
ELSEVIER
ANALYTICA
CHIMICA ACTA
AN INTERNATIONAL JOURNAL DEVOTED TO ALL BRANCHES OF ANALYTICAL CHEMISTRY
Editors:
Richard P. Baldwin
Wolfgang Buchberger
Lutgarde Buydens
Purnendu K. Dasgupta
Ulrich J. Krull
James P. Landers
Hian Kee Lee
Liang Li
Janusz Pawliszyn
Paul J. Worsfold
Review Editor:
Manuel Miró
ScienceDirect
makes sense.

This article appeared in a journal published by Elsevier. The attached copy is furnished to the author for internal non-commercial research and education use, including for instruction at the authors institution and sharing with colleagues.

Other uses, including reproduction and distribution, or selling or licensing copies, or posting to personal, institutional or third party websites are prohibited.

In most cases authors are permitted to post their version of the article (e.g. in Word or Tex form) to their personal website or institutional repository. Authors requiring further information regarding Elsevier's archiving and manuscript policies are encouraged to visit:

http://www.elsevier.com/copyright

Analytica Chimica Acta 664 (2010) 158–164

Contents lists available at ScienceDirect

Analytica Chimica Acta

journal homepage: www.elsevier.com/locate/aca

Modeling of electrokinetic transport in silica nanofluidic channels

Moran Wang [a,b,*], Qinjun Kang [a], Eli Ben-Naim [b]

[a] Computational Earth Science Group of Earth and Environmental Sciences Division, Los Alamos National Laboratory, Los Alamos, NM 87545, USA
[b] Physics of Condensed Matter and Complex Systems Group and Center for Nonlinear Study of Theoretical Division, Los Alamos National Laboratory, Los Alamos, NM 87545, USA

ARTICLE INFO

Article history:
Received 30 November 2009
Received in revised form 24 February 2010
Accepted 27 February 2010
Available online 6 March 2010

Keywords:
Electrokinetic transport
Nanofluidics
Surface dissociation
Double layer interaction

ABSTRACT

We present a theoretical and numerical modeling study of the multiphysicochemical process in electrokinetic transport in silica nanochannels. The electrochemical boundary condition is solved by considering both the chemical equilibrium on solid–liquid interfaces and the salt concentration enrichment caused by the double layer interaction. The transport behavior is modeled numerically by solving the governing equations using the lattice Poisson–Boltzmann method. The framework is validated by good agreements with the experimental data for all range of ionic concentrations. The modeling results suggest that when the double layers interact, the bulk salt concentration enrichment results in the saturation of conductances for low ionic concentrations. Both the streaming conductance and the electrical conductance are enhanced by the double layer interaction, and such enhancements diminish when the channel size is larger than 10 times of the Debye length. The streaming conductance increases with pH almost linearly when pH < 8, while the electrical conductance increases with pH exponentially.

Published by Elsevier B.V.

1. Introduction

Nanofluidics is an emerging field of interest because of its potential capabilities of controlling and manipulating fluids and inclusions (particles and ions) exquisitely [1–4], and its potential applications in biochemomedical analysis [5–9] and energy conversion systems [10–13]. Electrokinetic transport such as electroosmotic flows and streaming currents, known to be induced by charged surfaces of channels, is becoming increasingly arrestive and important at nanoscale because of the larger surface to volume ratio. New physical or chemical effects may arise as the electrical double layers (EDLs) interact in nanochannels [13–20]. Hibara et al. [16] reported lower dielectric constants and higher viscosities of the aqueous solution in nanometer-sized channels. Pu et al. [17] revealed the ion-enrichment and ion-depletion effects when a voltage was applied across a nanochannel. Stein et al. [2] and Karnik et al. [7] found that the electrical conductance of nanofluidic channels saturates at a value for the dilute electrolyte, which departs significantly from bulk behavior. This phenomenon was ascribed to the dominance of the effective surface-charge density [2,21,22]. Liu et al. [13] discovered that the apparent proton conductivity inside a nanochannel can be enhanced by orders of magnitude relative to that in a bulk solution, and such enhancement occurs even before EDLs overlap. Moreover, van der Heyden et al. [3] reported that the streaming current is approximately constant at low salt concentrations but drops at high-salt concentrations. Choi and Kim [23] modeled the streaming conductance of silica nanochannels using a self-consistent model and claimed that their predictions were more accurate than any models in the previous studies, however their models deviated significantly from the experimental data at the low concentration region. It is still a challenge to predict transport conductance that can agree well with the experimental data in both high and low ionic concentration regions [24]. Although some of these phenomena have been well investigated, a clear understanding of the underlying mechanisms for the surface-charge-governed electrokinetic transport in confined nanofluidics is still lacking.

This contribution focuses on the electrokinetic transports, both the electroosmotic flow and the streaming current, in silica nanofluidic channels through theoretical and numerical modeling. As the rapid developments of computational technology in recent years, the electrokinetic transport in nanofluidic channels has been investigated by both atomistic simulations [25–30] and continuum models [6,10,14,31,32]. It is still a major challenge now to predict the electrokinetic transport in channels using the first principle methods for a full range of ionic concentrations. In this study, we consider the nanochannels with an internal height in the range of 20–600 nm, which are commonly interested in nanofluidic devices. In this range, the continuum theories are still valid to describe the transport behavior because the size is much larger than the diameter of solvent molecules [33]; meanwhile the phenomena are significantly different from those in microfluidic devices due to the channel size comparable to the Debye length [1,6]. Another issue

---

* Corresponding author at: Computational Earth Science Group of Earth and Environmental Sciences Division, Los Alamos National Laboratory, Los Alamos, NM 87545, USA. Tel.: +1 505 664 0698; fax: +1 505 665-8737.
E-mail addresses: mwang@lanl.gov, moralwang@gmail.com (M. Wang).

0003-2670/$ – see front matter. Published by Elsevier B.V.
doi:10.1016/j.aca.2010.02.018

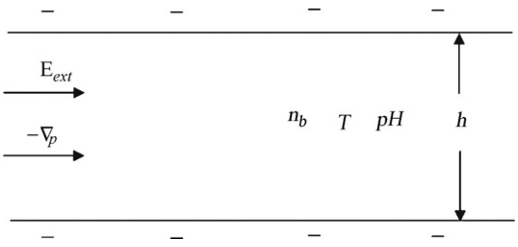

Fig. 1. Geometry and boundary conditions of a nanofluidic channel which is h high. T and pH are the local temperature and pH value, respectively, and n_b is the effective bulk ionic concentration. The electrolyte solution is driven flowing in the nanochannel either by an external electric field, $\mathbf{E}_{ext}$, or by a pressure gradient, $-\nabla p$.

we address in this work is the chemical dissociation and charge regulation of surfaces and their effects on the electric potential boundary conditions. In most of the previous numerical modeling of electrokinetic transport in nanochannels, either constant charge density [6,10,27,28,30,31], constant zeta potential [32], or chemical equilibrium condition [3,15] has been employed for the boundary condition on the wall surfaces. A recent study indicates that none of these result in good predictions compared with the experimental data [3]. Therefore, it is important to use better boundary conditions for modeling electrokinetic phenomena in nanofluidics [3]. The purpose of the present study is to develop a mathematical and numerical model to better predict the electrokinetic transport in nanofluidic channels for the entire region of ionic concentrations, and to reveal the physical and chemical transport mechanisms in nanofluidics, aiming to better design and optimize nanofluidic devices.

2. Mathematical models

2.1. Governing equations

In this work, we consider the electrokinetic transport in a two-dimensional (2D) straight smooth channel, as shown in Fig. 1. The channel is charged by the solid–liquid interaction. The channel is h high. The electrolyte solution is driven flowing in the nanochannel either by the external electric field, $\mathbf{E}_{ext}$, or by the pressure gradient, $-\nabla p$.

The mathematical models are based on the following assumptions: (i) the system is in chemical and dynamic equilibrium; (ii) the transport process is in steady state; (iii) the channel height is much larger than the solvent molecular size. As the thickness of the Stern layer (compact layer) is around one molecular diameter, depending on the ion-surface molecular interactions, it is negligible based on this large-enough-channel-height assumption; (iv) the ions in the Stern layer are attached on the surfaces and have no contribution to the bulk ionic current; (v) the bulk ionic concentration is not too high (<1 M) or too low so that the Poisson–Boltzmann (PB) model is still applicable [33]. When the bulk ionic concentration is higher than 1 M, the Boltzmann distribution will break down for ions due to the non-negligible volume fraction of ions and ions interactions [30]. On the other hand, if the bulk ionic concentration is very low for a given channel height so that the double layer thickness is greater than ten times of the channel height, the PB model will fails because of the double layer interactions compared with the Poisson–Nernst–Planck model [33] even if for the same boundary conditions; (vi) no other chemical reactions occur at surfaces except the dissociation of silanol groups. Under these assumptions, the governing equations for the electrokinetic transport in a nanochannel for a monovalent electrolyte solution are as follows [1,34,35]:

$$\nabla^2 \psi = \frac{2en_b}{\varepsilon\varepsilon_0} \sinh\left(\frac{e\psi}{kT}\right), \tag{1}$$

$$\rho_e = -2en_b \sinh\left(\frac{e\psi}{kT}\right), \tag{2}$$

$$\nabla \cdot \boldsymbol{u} = 0, \tag{3}$$

$$\rho\boldsymbol{u} \cdot \nabla\boldsymbol{u} = -\nabla p + \eta\nabla^2\boldsymbol{u} + \rho_e\boldsymbol{E}, \tag{4}$$

where ψ denotes the static electric potential, e the absolute value of proton charge, ε_0 the permittivity of vacuum, ε the relative dielectric constant of the solution, n_b the effective bulk ionic concentration, k the Boltzmann constant, T the absolute temperature, $\mathbf{u}$ the fluid velocity, ρ the fluid density, p the pressure, η the viscosity, ρ_e the charge density, and $\mathbf{E}$ the electric field strength. The electric field strength ($\mathbf{E}$) can be either the external electric field strength ($\mathbf{E}_{ext}$) for electroosmotic flows or the streaming induced electric field strength ($\mathbf{E}_{str}$) for pressure-driven flows which is often referred as the cause of the electroviscosity [36]. All the units are in or have to be converted to SI units for Eqs. (1)–(4).

2.2. Boundary conditions

As reported before [3], the boundary conditions are critical to modeling electrokinetic phenomena in nanofluidics. For the hydrodynamic boundary condition, we use the non-slip model at the silica surfaces. The slip boundary conditions have been adopted in some recent studies [37–39], and have shown significant effects on the ion transport in nanofluidics for some cases. However a careful molecular study showed that the hydrodynamic boundary condition, slip or not, depended on the molecular interactions between fluid and solid and on the channel size [40,41]. For the dilute solution in silica nanochannels considered in this work ($h \geqq 20$ nm), the non-slip boundary condition is still valid [29,42,43].

For the electrostatic boundary condition, in this work we use the Basic Stern (BS) model developed by Behrens and Grier [15] in which the silica surfaces acquire charges in contact with water by the dissociation of silanol groups [44]:

$$\mathrm{SiOH} \leftrightarrow \mathrm{SiO^-} + \mathrm{H^+}, \tag{5}$$

so that the diffusion layer potential (ζ) on the interface can be expressed as a function of the charge density (σ) [15]:

$$\zeta(\sigma) = \frac{kT}{e} \ln \frac{-\sigma}{e\Gamma + \sigma} - (\mathrm{pH} - \mathrm{pK})\frac{kT \ln\ 10}{e} - \frac{\sigma}{C} \tag{6}$$

where Γ is the surface density of chargeable sites, pK the logarithmic dissociation constant, and C the Stern layer's phenomenological capacity. Eq. (6) reflects the chemical nature of the silica–water interface and its charging process, however the BS model has some limitations: (i) hardly suitable for extremely acidic solutions (pH < 3) or for where the protonation of doubly coordinated groups ($\mathrm{Si_2}$–O) has to be taken into account [15,45]; (ii) unsuitable for high-salt-concentration solutions (>1 mM) since only silica–water interaction is considered [46].

For the flat surfaces of a nanochannel, the surface-charge density is approximated using the Grahame equation [47]:

$$\sigma(\zeta) = \frac{2\varepsilon\varepsilon_0 kT\kappa}{e} \sinh\left(\frac{e\zeta}{2kT}\right), \tag{7}$$

where κ^{-1} is the Debye screening length given by $\kappa = \sqrt{2z^2e^2n_b/\varepsilon\varepsilon_0 kT}$. Solving Eqs. (6) and (7) yields the electrostatic boundary conditions at the wall surfaces of the channels when the double layers do not interact. Such a chemical equilibrium boundary condition has been employed in the previous studies [3,19,48]. Fig. 2 shows the zeta potential on an isolated flat silica surfaces contacting with the NaCl solution. The solid line is predicted by the BS model and the circles are the experimental data from Gaudin and Fuerstenau [49]. The BS predictions agree with the experimental data in the dilute solutions (<1 mM). The BS model can be extended

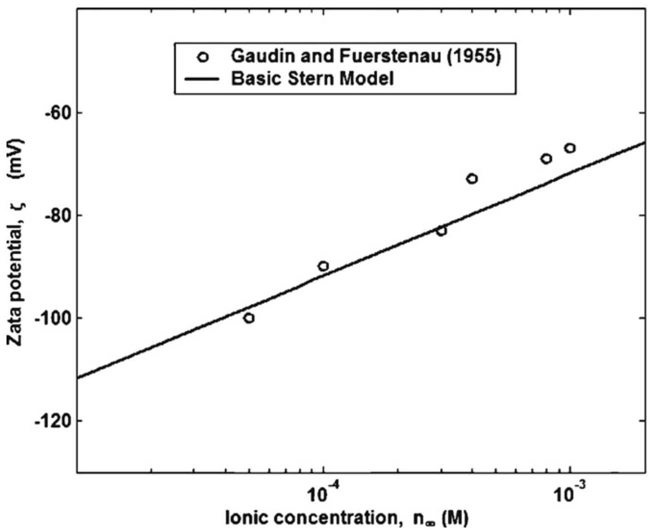

Fig. 2. Zeta potential versus bulk concentration for isolated flat silica surfaces. The cycles are from the experimental data from Gaudin and Fuerstenau [49]. The parameters using in the Basic Stern model are $\Gamma = 8\,\mathrm{nm}^{-2}$, $C = 2.9\,\mathrm{F\,m}^{-2}$ and pK 7.5 [15]. The other parameters are $T = 298$ K, and pH 6.5 [49].

to other non-silica materials, such as carbon and plastic materials, once the parameters (Γ, C, pK,) are given.

2.3. Effective bulk concentration

When the EDL interaction occurs in nanofluidic channels, a traditional “bulk” ionic concentration does not even exist. The local electroneutrality may be never obtained at the middle of channel for these cases. People have found the counter-ion-enrichment when the EDL overlap occurs in the nanochannels [17,20,30,50]. A few methods have been proposed to determine the effective bulk ionic concentration in nanochannels [19,51]. A reasonable determination for the effective bulk ionic concentration with double layer interactions in nanochannels requires (i) to reflect the dominating ions effects on transport and (ii) to transform to the traditional bulk concentration automatically when the double layer interaction vanishes. Based on these requirements, we present an enrichment coefficient, α, to calculate the effective bulk ionic concentration in this work, which is defined as

$$\alpha = \frac{n_{+,\mathrm{m}}}{n_\infty}, \tag{8}$$

where $n_{+,\mathrm{m}}$ represents the counter-ion concentration at the middle of the channel and n_∞ is the initial ionic concentration in the free-streaming flow. When the channel height is much larger than the Debye length, the effective bulk ionic concentration (n_b) equals to the initial (free-streaming) ionic concentration (n_∞). However if the channel height is comparable to the Debye length, the bulk ionic concentration at the middle of channel will be enriched by the interaction of double layers from both walls. Thus the effective bulk ionic concentration (n_b) is equal to $n_{+,\mathrm{m}}$ in value, and calculated by

$$n_\mathrm{b} = \alpha n_\infty. \tag{9}$$

The combination of Eqs. (1) and (6)–(9) yields a full description of the electrochemical boundary conditions even if the double layers interact in nanochannels. The solution process is as follows: (i) calculate the initial boundaries (ζ_0 and σ_0) using Eqs. (6) and (7) through iterations by assuming $n_\mathrm{b} = n_\infty$; (ii) solve the Poisson–Boltzmann equation, Eq. (1), using the initial boundary condition (ζ_0 or σ_0) to obtain the effective bulk concentration n_b; (iii) substitute n_b into Eqs. (6) and (7) and solve for the final boundary conditions (ζ and σ) through another iteration process.

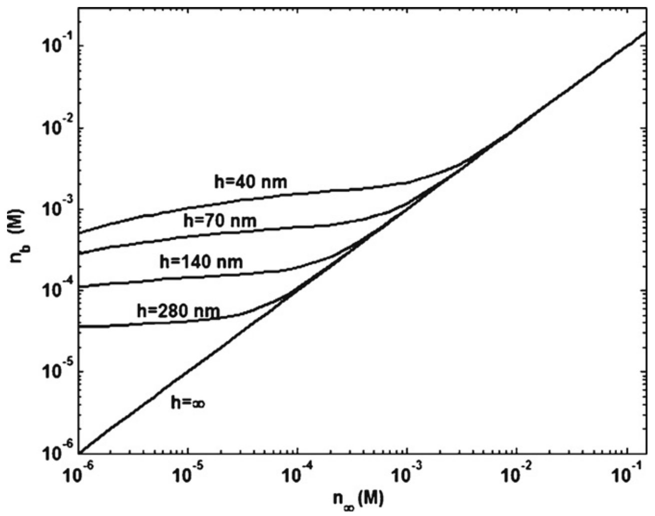

Fig. 3. Effective bulk concentration as a function of the initial bulk concentration for different channel heights (h). The chemical equilibrium parameters are $\Gamma = 8\,\mathrm{nm}^{-2}$, pK 7.9 and $C = 2.9\,\mathrm{F\,m}^{-2}$ from the reference [15]. The other parameters are $T = 293$ K and pH 8.

Fig. 3 shows the calculated effective bulk ionic concentration (n_b) as a function of the initial bath bulk concentration (n_∞) for different channel heights. For two isolated surfaces ($h = \infty$), n_b always equals n_∞. Once the double layers interact, n_b becomes greater than n_∞ and keeps approximately a constant in a wide range of n_∞. It decreases again slightly when the double layers interact very strongly (see the situation for $h = 40$ nm at $n_\infty = 10^{-6} \sim 10^{-5}$ M).

2.4. Simulation system and parameters

After the electrochemical boundary conditions are determined, the governing Eqs. (1)–(4) are solved numerically by a lattice Poisson–Boltzmann framework [52–54] in a 2D straight nanochannel. The lattice Poisson–Boltzmann method can be regarded as a highly efficient solver for the strongly nonlinear equations governing the multiphysical transport [52]. Different from the conventional computational methods for differential equations, the lattice evolution method employs the mesoscopic equations (for example, the Boltzmann equation) to determine macroscopic transport dynamics, and solves the governing equations by tracking the distribution functions of particle packets on lattices [55]. The lattice Poisson–Boltzmann framework includes an electric potential evolution method on discrete lattices to solve the nonlinear Poisson–Boltzmann equation and a density evolution method on the same set of discrete lattices to solve the Navier–Stokes equations [52,54]. This numerical framework was implemented in FORTRAN and has been validated with analytical solutions and experimental data for micro- and nanoscale electrokientic flows [52,54,56]. In the present work, we consider the flow of a KCl solution in a 2D silica nanofluidic channel either driven by a pressure gradient or by an external electric field. The channel height varies from 20 to 600 nm, the initial bulk KCl concentration from 10^{-6} to 1 M, and the pH value from 5 to 9. We use a 200 × 200 lattice system for most cases and refine the lattices when necessary to ensure that the lattice size is smaller than one third of the Debye length (κ^{-1}) for acceptable numerical accuracy. If the Debye length is smaller than 3% of the channel height, it satisfies the “thin layer” hypothesis and the electrokinetic transport can be simply calculated based on the Helmholtz–Smoluchowski model [1].

When the flow is driven by a pressure gradient, a streaming potential is established because of the ion transport. The streaming electric field is always opposite to the flow direction, and hence the net flow in the channel is diminished. This phenomenon is commonly referred as the electroviscosity effect since the liquid appears to be of higher viscosity near the surfaces [19,52,57]. In this work, the streaming electric field strength is calculated by a simplified model [57]

$$\boldsymbol{E}_{\mathrm{str}} = -\frac{\int_0^h \rho_{\mathrm{e}}\boldsymbol{u}\,dA}{A_{\mathrm{c}}\lambda_0 + P_{\mathrm{s}}\lambda_{\mathrm{s}}}, \tag{10}$$

where λ_0 is the electrical conductivity of the fluid, λ_{s} is the specific surface conductivity, A_{c} is the effective area of the channel's cross-section for the bulk conduction current and P_{s} the wetting parameter of the channel [58,59]

$$P_{\mathrm{s}} = 2(w + h), \tag{11}$$

where w is the channel width and h the channel height.

Although the fluid electrical conductivity (λ_0) depends on the electrolyte concentration and the surface-charge density [2,21] and the surface conductivity (λ_{s}) may vary with the channel size [59] and the ionic transport properties in the Stern layer [60], we use constant λ_0 and λ_{s} for simplification in this work at: $\lambda_0 = 1.42 \times 10^{-3}\ \Omega^{-1}\ \mathrm{m}^{-1}$ and $\lambda_{\mathrm{s}} = 1.64 \times 10^{-9}\ \Omega^{-1}$ [52,61].

The conductance is calculated after the numerical simulations and compared with the existing experimental data from the literature. For the pressure-driven flow, the streaming conductance is defined as the streaming current per unit applied pressure [3]

$$c_{\mathrm{str}} \equiv \frac{I_{\mathrm{str}}}{\Delta p} = \frac{1}{\Delta p}\int \rho_{\mathrm{e}}\boldsymbol{u}\,dS, \tag{12}$$

where I_{str} denotes the streaming current and S the cross-section area.

For the electroosmotic flow, the channel electrokinetic conductance is defined as the current per unit applied electrical potential difference [2]

$$c_{\mathrm{e}} \equiv \frac{I}{\Delta V} = \frac{1}{\Delta V}\left(\sum_i z_i e \int \mathbf{J}_i\,dS\right) \tag{13}$$

where the subscript i denotes the i-th ion species, and $\mathbf{J}$ the ionic flux determined by the Nernst–Planck equation [34,36,62]

$$\boldsymbol{J}_i = -\frac{ez_iD_i}{kT}n_i\nabla\psi + n_i\boldsymbol{u}, \tag{14}$$

where z is the valence and D the diffusivity of the ion. Another parameter, the ion mobility (μ_{m}), is often used to calculate the ionic current, defined as $\mu_{\mathrm{m},i} = ez_iD_i\ \mathrm{kT}^{-1}$. [2,63] The diffusivity and mobility of ion may vary with the ionic concentration. In this work, we assume constant ion properties since the mobility variance is within 0.3% when the ionic concentration is 10^{-6} ~1 M for the KCl solution [2].

The other simulation parameters, if not specified otherwise, are $\rho = 999.9\ \mathrm{kg\,m^{-3}}$, $\varepsilon\varepsilon_0 = 6.95 \times 10^{-10}\ \mathrm{C^2\,J^{-1}\,m}$, $\eta = 0.889\ \mathrm{mPa\,s}$, $T = 293\ \mathrm{K}$, $D_{\mathrm{K^+}} = 1.96 \times 10^{-9}\ \mathrm{m^2\,s^{-1}}$ and $D_{\mathrm{Cl^-}} = 2.03 \times 10^{-9}\ \mathrm{m^2\,s^{-1}}$. [6,53,56]

3. Results and discussion

3.1. Benchmark

To validate the present numerical framework, we first simulate the pressure-driven flow of a KCl solution in a silica nanochannel, calculate the streaming conductance, and compare with other models and experimental data [3]. Fig. 4 shows the results for a channel with $h = 140$ nm. The measured streaming conductance is for a three-dimensional rectangular channel with a high aspect ratio at about 360 [3]. It is expected that at such a high aspect ratio, the edge effects are negligible and the 2D simulations can result in a good approximation for the 3D experiments. We use $\zeta = -100$ mV for the constant zeta potential model and $\sigma = -10\ \mathrm{mC\,m^{-2}}$ for the constant charge density model. The electroviscosity effect is taken into account in the simulations for both models. The chemical equilibrium model solves the boundary condition only once, Eqs. (6) and (7), without the effective bulk concentration modification [3]. As a result, the streaming conductance calculated using this model does not fit the experimental data for low bulk concentrations ($<10^{-5}$ M), at which the bulk concentration-enrichment is substantial. The prediction for the constant surface-charge density deviates from the experimental data for low bulk concentrations due to the electroviscosity considered in our simulation. The result obtained from the present framework agrees much better than the other models with the experimental data in the entire concentration range, which increases sharply with the concentration decrease at high-salt concentrations, reaches the maximum at some moderate concentration, and keeps almost constant at low salt concentrations. Based on the present simulation process, it is reasonable to believe that the ionic concentration-enrichment caused by the EDL interaction results in the saturation of the surface-charge density and hence that of the streaming conductance. It is noticed that in Fig. 4 the present model still overrates the streaming conductance a little bit for low salt concentrations ($<10^{-4}$ M) even though they are within the error bars. One possible reason is that when the salt concentration is lower than 10^{-4} M, it is virtually hard to control pH due to the dissolved atmospheric CO_2 [64]. The pH of the solution will actually reduce from 8. The pH value effects on the transport properties of nanochannels will be discussed in the later part of this paper.

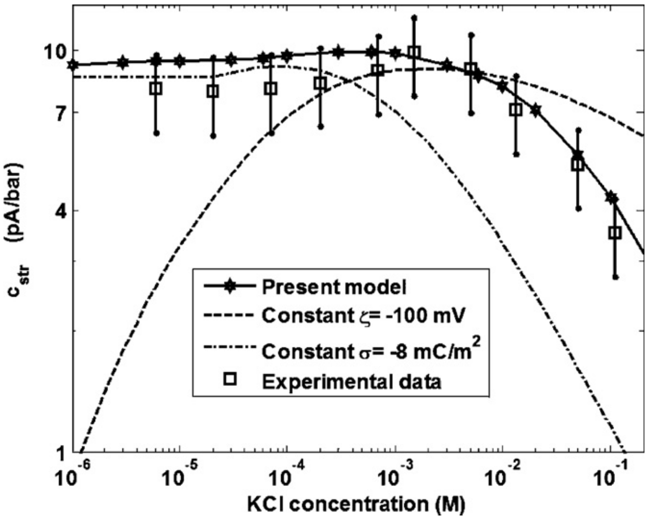

Fig. 4. Streaming conductance as a function of the initial bulk KCl concentration for a nanofluidic channel ($h = 140$ nm). The present simulation is compared with the constant zeta potential, constant charge density, the chemical equilibrium model and the experimental data from van der Heyden et al. [3]. The channel is 50 µm wide and 4.5 mm long [3]. The effective bulk ionic concentrations and zeta potentials in Fig. 1 are used for the present simulations.

3.2. Streaming conductance in pressure-driven flows

Fig. 5(a) shows the streaming conductance versus the initial KCl concentration for three different channels. The streaming conductance increases with the decrease of the KCl concentration, and then gets saturated after reaching a maximum value. The saturation conductance appears proportional to the channel size approximately. This result agrees well with the experimental observation qualitatively [3]. When all the results for different channel sizes

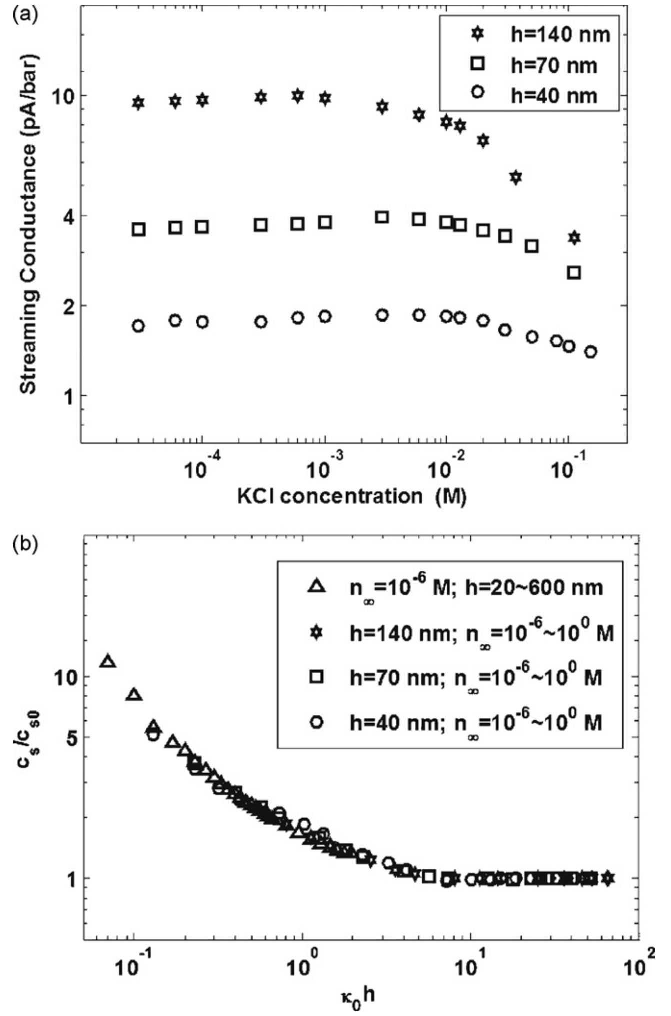

Fig. 5. Streaming conductance as a function of channel wall separations for KCl solutions at $T = 293$ K and pH 8. The other parameters are the same as those in Fig. 4.

(20–600 nm) and different salt concentrations are normalized, they fall into one curve as shown in Fig. 5(b). The streaming conductance c_s is normalized by c_{s0} which is based on the original chemical equilibrium model without the bulk concentration modification. The x axis is the dimensionless wall separation, $\kappa_0 h$, where κ_0 is calculated by the initial salt bulk concentration: $\kappa_0 = \sqrt{2z^2e^2n_\infty/\varepsilon\varepsilon_0 kT}$. The results indicates that the dimensionless streaming conductance increases with the decrease of the wall separation and is enhanced up to 10 times by the EDL interaction when the Debye length (κ_0^{-1}) is 10 times of the channel height (h). The effect from the EDL interaction fully diminishes and the dimensionless streaming conductance becomes a constant (unity) when the channel size is larger than 10 times of the Debye length.

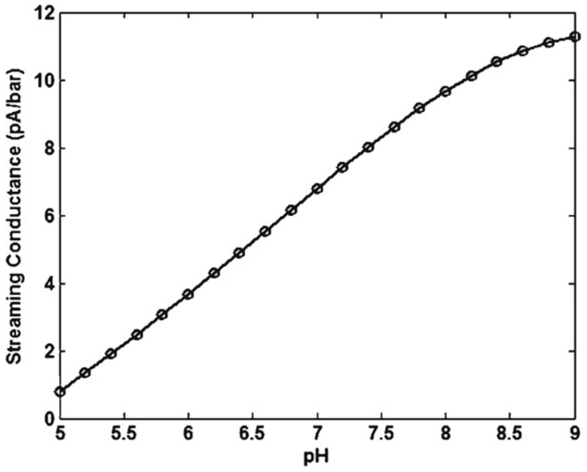

Fig. 6. Streaming conductance as a function of pH for KCl solutions at $T = 293$ K and $n_\infty = 10^{-4}$ M. The other parameters are the same as those in Fig. 4.

Fig. 6 shows pH effects on the streaming conductance for a 10^{-4} M KCl solution. The contribution from the buffer electrolyte, used to change the pH of the solution, is negligible in this pH range compared with the relative higher salt solution. Fig. 6 indicates that the streaming conductance increases with the increasing pH value almost linearly when pH < 8. This result suggests the streaming conductance sensitive to the pH value of the solution when pH < 8. Any decrease of pH of the dilute solution will lead to a remarkable decrease of the streaming conductance. This proves our hypothesis that the predictions will agree better with the experimental data in Fig. 4 at low ionic concentrations if the pH decrease caused by the dissolved CO_2 is taken into account [64].

3.3. Electrical conductance in electroosmotic flows

When an electrolyte solution is driven to flow in nanochannels by an external electric field, i.e. the electroosmotic flow,

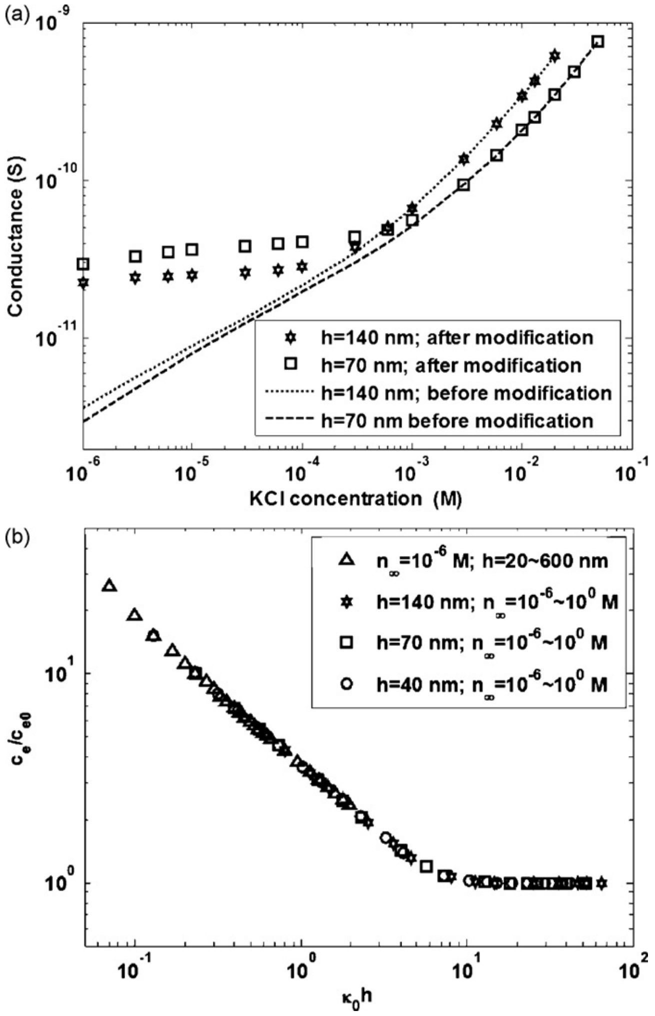

Fig. 7. Electrical conductance for different channel walls separations for KCl solutions at $T = 293$ K and pH 8. The other parameters are the same as those in Fig. 4.

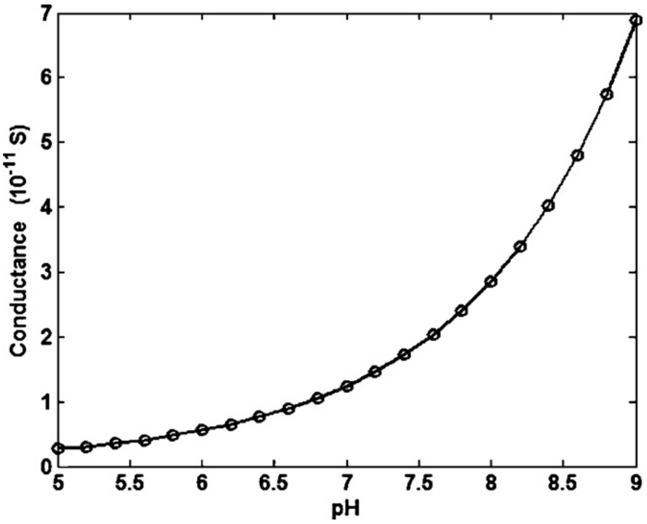

Fig. 8. Electrical conductance of a nanofluidic channel (h = 140 nm) as a function of pH for KCl solutions at T = 293 K and $n_\infty = 10^{-4}$ M. The other parameters are the same as those in Fig. 4. The inset displays a linear relationship when using a logarithmic y axis.

the electrical conductance becomes the most important quantity characterizing ion transport in the channels. Fig. 7(a) shows the electrical conductance as a function of the KCl concentration for two different channel sizes. The saturation phenomenon appears again, which is caused by the concentration-enrichment when the EDL overlap occurs and has been reported by experiments [2,7,13,21,22]. It is interesting to find that a larger channel has a higher conductance before the EDL overlap, but a lower conductance after that. Such a phenomenon has only been reported by Stein et al. [2] (see Fig. 2 in [2]). When we reformulate the conductance and the channel wall separation into dimensionless forms, the results fall into one curve, as shown in Fig. 7(b), for different channel sizes (20–600 nm) and salt concentrations (10^{-6} ~1 M). On a log-log plot, the dimensionless conductance changes linearly with the channel wall separation (dimensional channel size) in two regions. This prediction agrees well with the experimental data reported by Liu et al. [13] (see Fig. 4 in [12]). The conductance is enhanced nearly 20 times by the EDL interaction when the Debye length (κ_0^{-1}) is 10 times of the channel size (h), and similar with the streaming conductance, the effect from the EDL interaction diminishes when the channel size is larger than 10 times of the Debye length.

Fig. 8 shows the electrical conductance of a 140 nm nanochannel as a function of the pH value of a KCl solution at T = 293 K and $n_\infty = 10^{-4}$ M. The inset displays a linear relationship when using a logarithmic y axis, which indicates that the conductance increases with the pH value exponentially.

4. Conclusions

Electrokinetic transport in nanofluidic channels has been investigated using the present numerical framework. The electrochemical boundary condition is solved by considering both the chemical equilibrium on solid–liquid interfaces and the salt concentration-enrichment by the double layer interactions. The transport behavior is then simulated by solving the governing equations using the lattice Poisson–Boltzmann method. The channel size varies from 20 to 600 nm, the initial bulk concentration of KCl aqueous solution ranges from 10^{-6} to 1 M, and the pH value of the solution changes from 5 to 9. Both the streaming conductance for pressure-driven flows and the electrical conductance for electrically driven flows in nanochannels are calculated and compared with the existing experimental data. The following conclusions can be drawn from this study. (1) The bulk salt concentration-enrichment caused by double layer interactions plays the key role on the electrokinetic transport in nanofluidic channels when the double layer thickness is comparable to the channel height. The effective bulk concentration modification is based on the counter-ion concentration at the center of the channel. (2) Both the streaming conductance and the electrical conductance saturate when the EDLs interaction. The reason is the saturation of the surface-charge density and the zeta potential caused by the bulk salt concentration-enrichment. (3) Although the conductance varies with the channel size and the salt concentration, the normalized streaming conductance and electrical conductance versus the dimensionless channel wall separation falls into one curve, respectively, for given pH value and temperature of the solution. (4) Both the streaming conductance and the electrical conductance are enhanced about an order of magnitude by the EDL interaction when the Debye length (κ_0^{-1}) is 10 times of the channel size (h), and such effect fully diminishes when the channel size is larger than 10 times of the Debye length. (5) The streaming conductance increases with the pH value approximately linearly when $\mathrm{pH} < 8$, while the electrical conductance increases with the pH value at an exponential rate.

Acknowledgement

This work is supported by LANL's LDRD Project 20080727PRD2, through the J.R. Oppenheimer Fellowship awarded to M.W. The authors would like to thank Prof. Stein D for providing the experimental data, Prof. Dekker C., Prof. Yang R.J., Dr. Lichtner P., Prof. Revil A. and Prof. Bazant M. for helpful discussions.

References

[1] R.B. Schoch, J.Y. Han, P. Renaud, Reviews of Modern Physics 80 (2008) 839.
[2] D. Stein, M. Kruithof, C. Dekker, Physical Review Letters 93 (2004) 035901.
[3] F.H.J. van der Heyden, D. Stein, C. Dekker, Physical Review Letters 95 (2005) 116104.
[4] B. Bourlon, J. Wong, C. Miko, L. Forro, M. Bockrath, Nature Nanotechnology 2 (2007) 104.
[5] D. Stein, F.H.J. van der Heyden, W.J.A. Koopmans, C. Dekker, Proceedings of the National Academy of Sciences of the United States of America 103 (2006) 15853.
[6] H. Daiguji, P.D. Yang, A. Majumdar, Nano Letters 4 (2004) 137.
[7] R. Karnik, K. Castelino, R. Fan, P. Yang, A. Majumdar, Nano Letters 5 (2005) 1638.
[8] H. Chang, F. Kosari, G. Andreadakis, M.A. Alam, G. Vasmatzis, R. Bashir, Nano Letters 4 (2004) 1551.
[9] X.Y. Wang, S.L. Wang, B. Gendhar, C. Cheng, C.K. Byun, G.B. Li, M.P. Zhao, S.R. Liu, Trac-Trends in Analytical Chemistry 28 (2009) 64.
[10] H. Daiguji, P.D. Yang, A.J. Szeri, A. Majumdar, Nano Letters 4 (2004) 2315.
[11] F.H.J. van der Heyden, D.J. Bonthuis, D. Stein, C. Meyer, C. Dekker, Nano Letters 6 (2006) 2232.
[12] F.H.J. van der Heyden, D.J. Bonthuis, D. Stein, C. Meyer, C. Dekker, Nano Letters 7 (2007) 1022.
[13] S.R. Liu, Q.S. Pu, L. Gao, C. Korzeniewski, C. Matzke, Nano Letters 5 (2005) 1389.
[14] W.L. Qu, D.Q. Li, Journal of Colloid and Interface Science 224 (2000) 397.
[15] S.H. Behrens, D.G. Grier, Journal of Chemical Physics 115 (2001) 6716.
[16] A. Hibara, T. Saito, H.B. Kim, M. Tokeshi, T. Ooi, M. Nakao, T. Kitamori, Analytical Chemistry 74 (2002) 6170.
[17] Q.S. Pu, J.S. Yun, H. Temkin, S.R. Liu, Nano Letters 4 (2004) 1099.
[18] A. Plecis, R.B. Schoch, P. Renaud, Nano Letters 5 (2005) 1147.
[19] K.D. Huang, R.J. Yang, Nanotechnology 18 (2007) 115701.
[20] G.B. Li, S.L. Wang, C.K. Byun, X.Y. Wang, S.R. Liu, Analytica Chimica Acta 650 (2009) 214.
[21] R.B. Schoch, P. Renaud, Applied Physics Letters 86 (2005) 253111.
[22] H.C. Chang, G. Yossifon, Biomicrofluidics 3 (2009) 012001.
[23] Y.S. Choi, S.J. Kim, Journal of Colloid and Interface Science 333 (2009) 672.
[24] C.C. Chang, R.J. Yang, Journal of Colloid and Interface Science 339 (2009) 517.
[25] A.P. Thompson, Journal of Chemical Physics 119 (2003) 7503.
[26] W. Zhu, S.J. Singer, Z. Zheng, A.T. Conlisk, Physical Review E 71 (2005).
[27] R. Qiao, N.R. Aluru, Physical Review Letters 92 (2004) 198301.
[28] R. Qiao, J.G. Georgiadis, N.R. Aluru, Nano Letters 6 (2006) 995.
[29] M. Wang, J. Liu, S. Chen, Molecular Simulation 33 (2007) 239.
[30] M. Wang, J. Liu, S. Chen, Molecular Simulation 33 (2007) 1273.
[31] H.S. White, A. Bund, Langmuir 24 (2008) 2212.

[32] S. Pennathur, J.G. Santiago, Analytical Chemistry 77 (2005) 6772.
[33] M. Wang, S.Y. Chen, Communications in Computational Physics 3 (2008) 1087.
[34] D.Q. Li, Encyclopedia of Microfluidics and Nanofluidics, Springer Verlag, New York, 2008.
[35] S.H. Behrens, M. Borkovec, Physical Review E 60 (1999) 7040.
[36] V.G. Levich, Physico-Chemical Hydrodynamics, Prentice-Hall, New York, 1962.
[37] C. Davidson, X.C. Xuan, Journal of Power Sources 179 (2008) 297.
[38] Y.Q. Ren, D. Stein, Nanotechnology 19 (2008).
[39] S. Pennathur, J.C.T. Eijkel, A. van den Berg, Lab on a Chip 7 (2007) 1234.
[40] J.F. Dufreche, V. Marry, N. Malikova, P. Turq, Journal of Molecular Liquids 118 (2005) 145.
[41] L. Joly, C. Ybert, E. Trizac, L. Bocquet, Physical Review Letters 93 (2004) 4.
[42] C.D. Lorenz, P.S. Crozier, J.A. Anderson, A. Travesset, Journal of Physical Chemistry C 112 (2008) 10222.
[43] R. Qiao, N.R. Aluru, Applied Physics Letters 86 (2005).
[44] J. Westall, H. Hohl, Advances in Colloid and Interface Science 12 (1980) 265.
[45] T. Hiemstra, J.C.M. Dewit, W.H. Vanriemsdijk, Journal of Colloid and Interface Science 133 (1989) 105.
[46] M. Wang, A. Revil, Journal of Colloid and Interface Science 343 (2010) 381.
[47] F. Baldessari, Journal of Colloid and Interface Science 325 (2008) 526.
[48] B.T. Hughes, J.M. Berg, D.L. James, A. Ibraguimov, S.R. Liu, H. Temkin, Microfluidics and Nanofluidics 5 (2008) 761.
[49] A.M. Gaudin, D.W. Fuerstenau, Transactions of the American Institute of Mining and Metallurgical Engineers 202 (1955) 66.
[50] L.J. Cheng, L.J. Guo, Nano Letters 7 (2007) 3165.
[51] R. Qiao, N.R. Aluru, International Journal for Multiscale Computational Engineering 2 (2004) 173.
[52] J.K. Wang, M. Wang, Z.X. Li, Journal of Colloid and Interface Science 296 (2006) 729.
[53] M. Wang, Q. Kang, Analytical Chemistry 81 (2009) 2953.
[54] M.R. Wang, J.K. Wang, S.Y. Chen, Journal of Computational Physics 226 (2007) 836.
[55] S. Chen, G.D. Doolen, Annual Review of Fluid Mechanics 30 (1998) 329.
[56] M. Wang, S. Chen, Journal of Colloid and Interface Science 314 (2007) 264.
[57] D.Q. Li, Electrokinetics in Microfluidics, Academic, Oxford, 2004.
[58] D.Q. Li, Colloids and Surfaces A: Physicochemical and Engineering Aspects 195 (2001) 35.
[59] L.Q. Ren, D.Q. Li, W.L. Qu, Journal of Colloid and Interface Science 233 (2001) 12.
[60] J. Lyklema, Journal of Physics: Condensed Matter 13 (2001) 5027.
[61] B. Li, D.Y. Kwok, The Journal of Chemical Physics 120 (2004) 947.
[62] P.C. Lichtner, Material Research Society Symposium Proceedings 353 (1995) 117.
[63] S. Levine, J.R. Marriott, K. Robinson, Journal of the Chemical Society-Faraday Transactions II 71 (1975) 1.
[64] A. Persat, R.D. Chambers, J.G. Santiago, Lab on a Chip 9 (2009) 2437.